Unconventional iron-magnesium compounds at terapascal pressures

Yimei Fang,[1] Yang Sun,[2,*] Renhai Wang,[3,4] Feng Zheng,[1] Shunqing Wu,[1,†] Cai-Zhuang Wang,[4] Renata M. Wentzcovitch,[2,5,6,‡] and Kai-Ming Ho[4]

[1]*Department of Physics, OSED, Key Laboratory of Low Dimensional Condensed Matter Physics (Department of Education of Fujian Province), Jiujiang Research Institute, Xiamen University, Xiamen 361005, China*

[2]*Department of Applied Physics and Applied Mathematics, Columbia University, New York, New York 10027, USA*

[3]*School of Physics and Optoelectronic Engineering, Guangdong University of Technology, Guangzhou 510006, China*

[4]*Department of Physics, Iowa State University, Ames, Iowa 50011, USA*

[5]*Department of Earth and Environmental Sciences, Columbia University, New York, New York 10027, USA*

[6]*Lamont-Doherty Earth Observatory, Columbia University, Palisades, New York 10964, USA*

(Received 15 April 2021; revised 12 October 2021; accepted 14 October 2021; published 26 October 2021)

Being a lithophile element at ambient pressure, magnesium has been long believed to be immiscible with iron. Authors of a recent study showed that pressure turns magnesium into a siderophile element and can produce unconventional Fe-Mg compounds [Gao *et al.*, New J. Chem. **43**, 17403 (2019)]. Here, we extend the investigation to exoplanetary pressure conditions using an adaptive genetic algorithm-based variable-composition structural prediction approach. We identify several Fe-Mg phases up to 3 TPa at 0 K. Our cluster alignment analysis reveals that most of the predicted Fe-Mg compounds prefer a body-centered cubic packing motif at terapascal pressures. In this paper, we provide a more comprehensive structure database to support future investigations of the high-pressure structural behavior of Fe-Mg and ternary, quaternary, etc. compounds involving these elements.

DOI: 10.1103/PhysRevB.104.144109

I. INTRODUCTION

For systems with significant atomic size mismatch at ambient conditions, limited solid intersolubility is observed. One such system is the Fe-Mg binary alloy. Previous results showed that <1273 K, Mg does not dissolve in Fe, while at the liquidus temperature, the maximum solubility of Mg in δ-Fe [the high-temperature Fe allotrope with body-centered cubic (bcc) structure] only reaches 0.25 at. % [1]. Some attempts have been made to facilitate Fe-Mg interalloying using ion-beam mixing [2] or mechanical alloying [3]. Additionally, several studies have shown that high pressures can improve the Fe-Mg intersolubility. At 20 GPa and 2273 K, Dubrovinskaia *et al.* [4] achieved a homogeneous Fe-Mg alloy with 4 at. % Mg. Later on, the same authors observed a significantly improved solubility of Mg (>10 at. %) in Fe at 126(3) GPa and 3650(250) K [5]. The authors ascribed the improved Fe-Mg intersolubility to the dramatic atomic size difference reduction under pressure [5].

There are also various theoretical investigations on the possibility of Fe-Mg interalloying under Earth's core conditions. Kadas *et al.* [6] demonstrated that Mg plays an essential role in the dynamical stability of bcc Fe and that a bcc structured Fe-Mg alloy with 5–10 at. % Mg reproduces the physical properties of Earth's inner core very well. Li *et al.* [7] found that solid Fe can incorporate substantial amounts of Mg at 360 GPa and 6500 K. More recently, Gao *et al.* [8] predicted a series of stable Fe-Mg compounds with different stoichiometries under pressures up to 360 GPa. An analysis of the electron localization function and density of states (DOS) of these Fe-Mg compounds indicated that the electron transfer from Mg to Fe helps the formation of Fe-Mg compounds at high pressures [8]. These theoretical findings suggest that Mg is a likely light element in the Earth's solid core.

To date, limited studies have reported the formation of Fe-Mg compounds under exoplanetary interior pressures. Here, we perform an adaptive genetic algorithm (AGA)-based structure prediction of the binary Fe-Mg phase diagram at 1, 2, and 3 TPa. Several unexpected compounds, i.e., Fe_2Mg, FeMg, $FeMg_2$, and $FeMg_3$ are found to be stable. By exploring the local packing motifs of stable and metastable compounds, we find the bcc packing motif is favored at high pressure. In this paper, we focus on structural and motif information. Temperature effects on the stability of found phases will be addressed in a future study.

In the following section, we describe the computational details of the structural prediction method and the density functional theory (DFT) calculations. Section III shows the identified phases and their stability, as well as discussions of the results. Conclusions are presented in Sec. IV

II. COMPUTATIONAL METHODS

The structural prediction of Fe-Mg compounds was carried out using an AGA which offers a balance between the speed of structure exploration with classical potentials and the accuracy of DFT calculation in an iterative way. The initial

*ys3339@columbia.edu
†wsq@xmu.edu.cn
‡rmw2150@columbia.edu

candidate structure pool in the genetic algorithm (GA) search was generated by randomly creating 128 structures without any assumption on the lattice symmetry. The structures were then relaxed to the nearest local minima and ranked by their enthalpies. In each GA generation, 32 structures, i.e., $\frac{1}{4}$ of the pool size, were produced from the parent structure pool through the mating procedure described in Ref. [9]. These structures replaced the worst 32 structures in the pool to form another generation of structures. We performed structure searches for 600 consecutive GA generations under each set of auxiliary interatomic potential. After the GA search cycle, 16 lowest-enthalpy structures were selected for DFT calculations to produce enthalpies, forces, and stresses for readjusting the classical auxiliary potential parameters for the next GA search. A total of 40 adaptive iterations were performed to obtain the final structures for the given chemical composition. Here, the classical auxiliary potential was determined by the embedded-atom method (EAM) [10] based on interatomic potentials. Within the EAM, the total energy of an N-atom system has the form

$$E_{\text{total}} = \frac{1}{2}\sum_{i,j(i\neq j)}^{N}\phi(r_{ij}) + \sum_{i}F_i(n_i), \tag{1}$$

where $\phi(r_{ij})$ denotes the pair repulsion between atoms i and j with a distance of r_{ij}, and $F_i(n_i)$ is the embedded term with electron density term $n_i = \sum_{j\neq i}\rho_j(r_{ij})$ at the site occupied by atom i. The fitting parameters in the EAM formula for the Fe-Mg system are determined as follows: the Lennard-Jones function modeled the parameters for Fe-Fe, Fe-Mg, and Mg-Mg interactions

$$\phi(r_{ij}) = 4\varepsilon\left[\left(\frac{\sigma}{r_{ij}}\right)^{12} - \left(\frac{\sigma}{r_{ij}}\right)^{6}\right], \tag{2}$$

where ε and σ are the fitting parameters. For Fe and Mg atoms, the density function was modeled by an exponentially decaying function

$$\rho(r_{ij}) = \alpha\exp\left[-\beta(r_{ij} - r_0)\right], \tag{3}$$

where α and β are fitting parameters, and the embedding function takes the form proposed by Banerjea and Smith in Ref. [11] as follows:

$$F(n) = F_0[1 - \gamma\ln n]n^{\gamma}, \tag{4}$$

where F_0 and γ are fitting parameters. During the AGA run, the fitting parameters were adjusted adaptively in light of the DFT calculated enthalpies, forces, and stresses of selected structures. The fitting procedure was realized using the force-matching method with the stochastic simulated annealing algorithm implemented in the POTFIT code [12,13].

The first-principles calculations were carried out utilizing the QUANTUM ESPRESSO code [14,15]. The exchange-correlation functional was treated with the non-spin-polarized generalized-gradient approximation and parameterized by the Perdew-Burke-Ernzerhof formula. The pseudopotentials for Fe and Mg were generated, tested, and previously used, e.g., in Ref. [16]. The pseudopotential for Fe was generated with the valence electronic configuration of $3s^2 3p^6 3d^{6.5} 4s^1$. Core radii for all quantum numbers l were 1.8 a.u. Five configurations $3s^2 3p^0$, $3s^1 3p^1$, $3s^1 3p^{0.5} 3d^{0.5}$, $3s^1 3p^{0.5}$, and $3s^1 3d^1$ with decreasing weights 1.5, 0.6, 0.3, 0.3, and 0.2, respectively, were used for Mg. Core radii for all quantum numbers l were 2.5 a.u. The pseudopotentials were also previously used in a few studies at terapascal pressures [17,18]. A kinetic-energy cutoff of 50 Ry for wave functions and 500 Ry for potentials were used. The cutoff energy of 50 Ry is fine enough to achieve convergence in the total energy, and the same value is adopted by a number of previous works [16,19,20]. Brillouin-zone integration was performed over the k-point grid of $2\pi \times 0.03$ Å^{-1} in the structure refinement. The convergence thresholds were 0.01 eV/Å for the atomic force, 0.5 kbar for the pressure, and 1×10^{-5} eV for the total energy. The structural optimization was performed under constant pressure using the Broydon-Fletcher-Goldfarb-Shanno algorithm [21–25] with variable cell shapes. The calculations of phonon spectra were carried out using the finite displacement approach as implemented in the PHONOPY code [26,27].

III. RESULTS AND DISCUSSION

A. Phase stability

To obtain low-enthalpy structures in the Fe-Mg system, we performed an extensive search in the compositional space of Fe_xMg_y ($x, y = 1$–4) with maximum simulation cells containing up to 32 atoms at pressures of 1, 2, and 3 TPa. The thermodynamic stability of Fe_xMg_y compounds was assessed by computing the formation enthalpies from the enthalpies of the elementary Fe and Mg in their stable phases at the same pressures. Specifically, the enthalpy of formation per atom (H_f) for a Fe_xMg_y phase is obtained as

$$H_f = \frac{H_{Fe_xMg_y} - (xH_{Fe} + yH_{Mg})}{x + y}. \tag{5}$$

Both elementary Fe and Mg exhibit multiple allotropes under pressure [28–31]. Experimental and theoretical efforts have established their phase diagrams. Here, the simple hexagonal (sh)-structured Mg and hexagonal close-packed (hcp) Fe ground states are used as references at 1 TPa. The simple cubic (sc) Mg and hcp Fe are used as references at 2 and 3 TPa. Figure 1(a) depicts the convex hulls of the Fe-Mg system constructed using H_f. It is shown that four stoichiometric Fe_xMg_y phases, i.e., Fe_2Mg, FeMg, $FeMg_2$, and $FeMg_3$ are thermodynamically stable.

We construct the pressure-composition phase diagram in Fig. 1(b) from 360 GPa, the upper limit for the pressure considered in Ref. [8], to 3 TPa (i.e. 3000 GPa). One observes that $FeMg_3$ and Fe_2Mg become unstable >1590 GPa and 1625 GPa, respectively. $FeMg_2$ has two stable phases within the pressure range of our interest, with the phase transition occurring at 2241 GPa. At pressures <675 GPa, FeMg has a stable phase with $Fd\bar{3}m$ symmetry, while at pressures >976 GPa, it stabilizes in a cubic lattice with $Pm\bar{3}m$ symmetry. All crystallographic parameters of the stable structures are listed in Table S1 in the Supplemental Material [32].

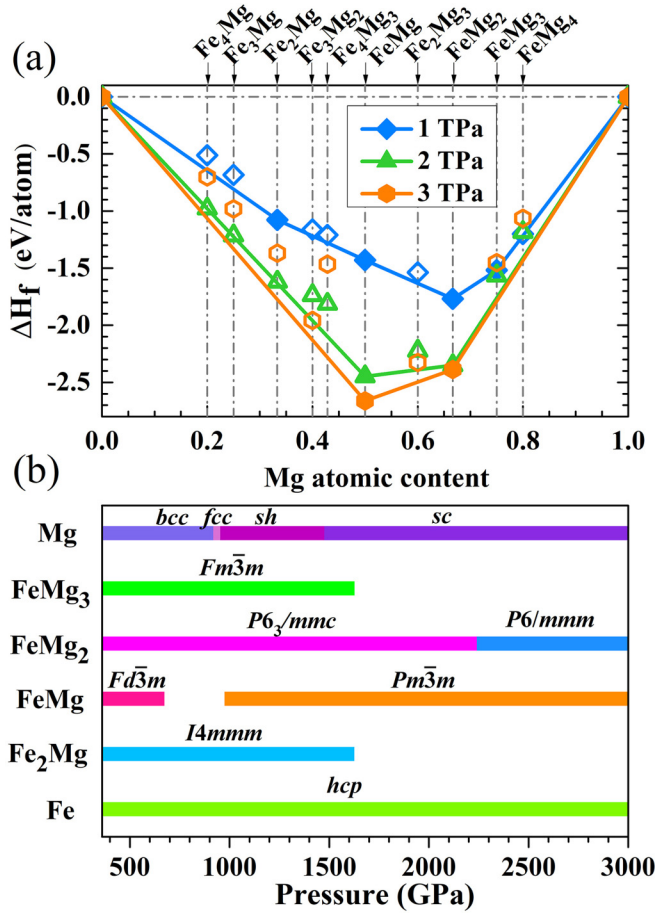

FIG. 1. Stability of Fe-Mg compounds. (a) Convex hull diagrams of the Fe-Mg compounds at exoplanetary pressures. Solid symbols represent the ground states, while open symbols denote the metastable phases. The convex hulls are shown by solid lines that connect ground states. (b) Pressure-composition phase diagram of the Fe-Mg system.

B. Geometries and phonon stabilities

1. Fe_2Mg

This Fe-rich phase forms a tetragonal structure with $I4/mmm$ symmetry [Fig. 2(a)], which is the standard ground-state structure of binary compounds with A_2B stoichiometry at high pressures, e.g., Fe_2O [33] and Al_2S [34]. In this structure, both Fe and Mg locate at the centers of the face-shared cube, but the difference is that each Fe is coordinated to 4 Fe and 4 Mg, while each Mg is bonded to 8 Fe [Figs. 2(b) and 2(c)]. Interestingly, this structure was found to be stable from 220 to 360 GPa by Gao *et al.* [8]. Here, we show that it can withstand high pressures up to 1625 GPa. At higher pressures, it will decompose into FeMg and Fe, as shown in the convex hull diagrams for 2 and 3 TPa in Fig. 1(a). The phonon spectrum shown in Fig. 2(d) confirms that it is dynamically stable at 1 TPa with an electron temperature (T_{el}) of 8000 K. Generally, the temperature at the core-mantle boundary of a super-Earth falls within the range from 4000 to 10 000 K [35]. Therefore, $T_{el} = 8000$ K is a reasonable choice. Nevertheless, the phonon spectra with $T_{el} = 0$ and 3000 K are also presented in Fig. S1 in the Supplemental Material [32], showing no imaginary frequencies in the entire Brillouin zone.

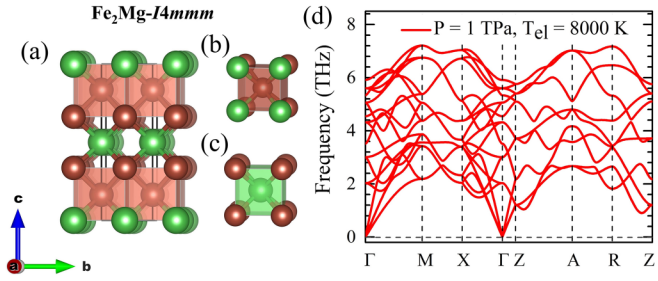

FIG. 2. (a) Crystal structure of $I4/mmm$ Fe_2Mg at 1 TPa. Fe and Mg atoms are indicated by brown and green balls, respectively. (b) Fe-centered and (c) Mg-centered coordination polyhedra. (d) Phonon dispersion of $I4/mmm$ Fe_2Mg at 1 TPa.

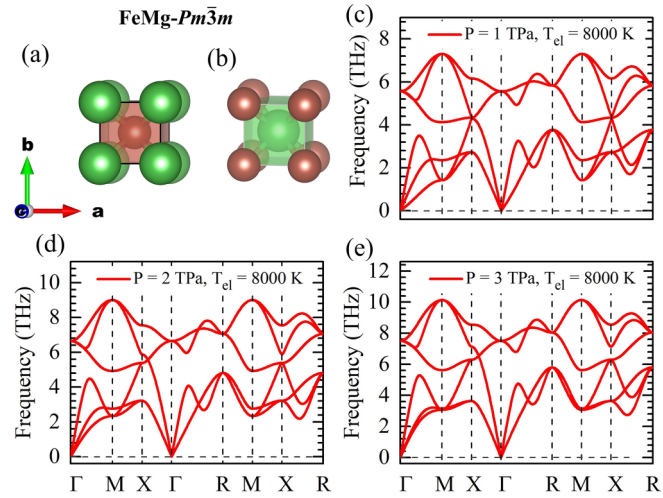

FIG. 3. (a) Crystal structure of $Pm\bar{3}m$ FeMg. Fe and Mg atoms are indicated by brown and green balls, respectively. (b) Mg-centered coordination polyhedra. (c)–(e) Phonon spectra of $Pm\bar{3}m$ FeMg at 1, 2, and 3 TPa, respectively.

2. FeMg

From 360 to 675 GPa, the $Fd\bar{3}m$ phase previously identified in Ref. [8] is the ground state. The $Fd\bar{3}m$ phase has a bcc-like crystal structure such that each atom has 50% of the nearest neighbor sites occupied by atoms of the same kind. From 976 GPa to 3 TPa, we find FeMg transform into the CsCl-type (B2) structure with $Pm\bar{3}m$ symmetry [see Fig. 3(a)]. In the pressure range from 675 to 976 GPa, FeMg decomposes to $FeMg_2$ and Fe_2Mg, which leaves a gap in the stability bar shown in Fig. 1(b). The dynamic stability of $Pm\bar{3}m$ FeMg at 1, 2, and 3 TPa is verified by the absence of imaginary frequencies in the phonon dispersion, as shown in Figs. 3(c)–3(e). Phonon dispersions with $T_{el} = 0$ and 3000 K are shown in Fig. S2 in the Supplemental Material [32].

3. $FeMg_2$

$FeMg_2$ adopts the hexagonal $P6_3/mmc$ structure at 1 and 2 TPa [see Fig. 4(a)]. Each Fe in this phase is coordinated by 5 Mg, forming a Fe-centered face-sharing tetrahedron, as shown in Fig. 4(b). While half of Mg forms the same

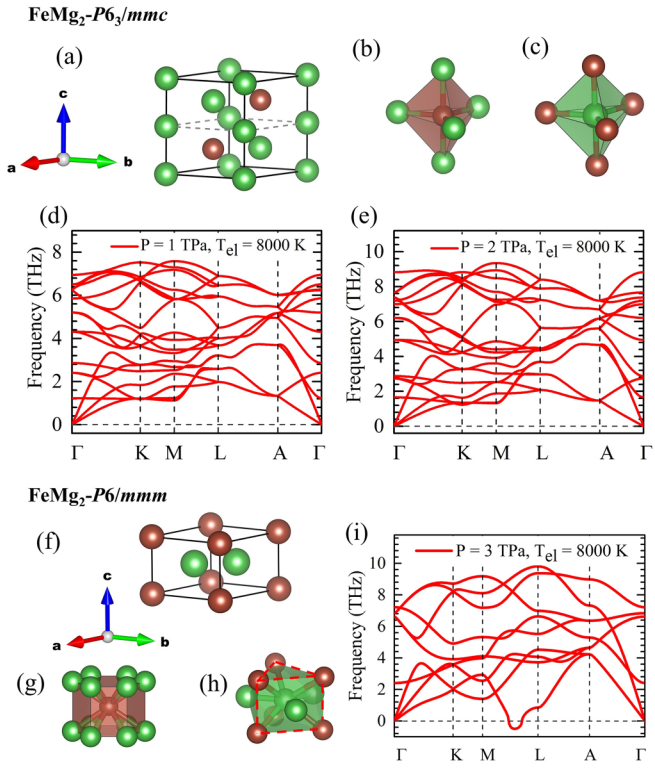

FIG. 4. (a) Crystal structure of $P6_3/mmc$ $FeMg_2$ at 1 and 2 TPa. Fe and Mg atoms are indicated by brown and green balls, respectively. The dashed line indicates the lattice analogous to the well-known ω phase. (b) Fe-centered and (c) Mg-centered coordination polyhedra. (d) and (e) Phonon dispersions of $P6_3/mmc$ $FeMg_2$ at 1 and 2 TPa, respectively. (f) Crystal structure of $P6/mmm$ $FeMg_2$ at 3 TPa. (g) Fe-centered and (h) Mg-centered coordination polyhedra, red dashed lines indicate a prismatic wedge. (i) Phonon dispersion of $P6/mmm$ $FeMg_2$ at 3 TPa.

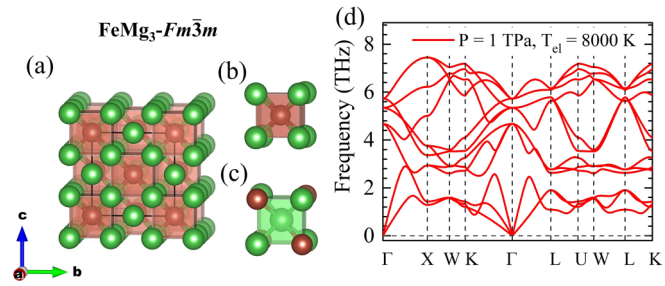

FIG. 5. (a) Crystal structure of $Fm\bar{3}m$ $FeMg_3$ at 1 TPa. Fe and Mg atoms are indicated by brown and green balls, respectively. (b) Fe-centered and (c) Mg-centered coordination polyhedra. (d) Phonon dispersion of $Fm\bar{3}m$ $FeMg_3$ at 1 TPa.

polyhedra as Fe [see Fig. 4(c)], the remaining half of Mg forms an isolated chain along the z direction. At 2241 GPa, the $P6_3/mmc$-$FeMg_2$ transforms into a AlB_2-type hexagonal structure with $P6/mmm$ symmetry, as shown in Fig. 4(f). Fe atoms are coordinated with 12 Mg atoms to form $FeMg_{12}$ polyhedra in hexagonal prisms [see Fig. 4(g)], while Mg atoms are coordinated with 6 Fe atoms and 3 Mg atoms to form trigonal prisms with Mg embedded in the side faces [see Fig. 4(h)]. Both $P6_3/mmc$ and $P6/mmm$ show a motif analogous to the well-known ω phase which is adopted in many elemental transition metals [36–39]. The main difference between $P6_3/mmc$ and $P6/mmm$ is the site occupations of Fe and Mg [see Figs. 4(a) and 4(f)]. Phonon calculations show that the $P6_3/mmc$-$FeMg_2$ is dynamically stable at pressures from 1 to 3 TPa and electronic temperatures from 0 to 8000 K (see Figs. 4(d) and 4(e) and S3 in the Supplemental Material [32]). Here, $P6/mmm$ is more thermodynamically stable than $P6_3/mmc$ at 3 TPa. Its phonon spectrum is stable at $T_{el} = 0$ and 3000 K (Fig. S4 in the Supplemental Material [32]). However, an imaginary frequency appears at $T_{el} = 8000$ K, shown in Fig. 4(i). When further increasing the electronic temperature, we find this imaginary phonon leads to a phase transition from the current $P6/mmm$ phase to a bcc-like $I4/mmm$ phase via a shear motion (see Fig. S5 in the Supplemental Material [32]). Thermodynamically, the transition only happens with ultrahigh electronic temperatures (Fig. S6 in the Supplemental Material [32]). Therefore, the $P6/mmm$ phase is still the ground state at 3 TPa. It is interesting to note that this transition is similar to the ω-bcc phase transitions found in transition-metal alloys such as Ti and Zr, where ω is stable at low temperature, while bcc is only stable at high temperatures [36,37]. The ω-bcc phase transition can also be understood from the DOS of these $FeMg_2$ phases. As shown in Fig. S7 in the Supplemental Material [32], the bcc-like phase has more states than $P6_3/mmc$ and $P6/mmm$ phases around the Fermi level at $T_{el} = 8000$ K, suggesting that the entropic stabilization is larger for the bcc-like phase. Such large electronic entropy lowers the enthalpy, therefore increasing the stability of the bcc-like phase at high temperatures (see Fig. S6 in the Supplemental Material [32]). We note the anharmonic effect is not included in this paper, and it is likely to further stabilize the bcc-like phase at high temperatures [40].

4. $FeMg_3$

This phase exhibits a cubic structure with $Fm\bar{3}m$ symmetry. It is composed of face-shared cubes with Fe/Mg being the central atoms, as shown in Figs. 5(a)–5(c). It was reported that $Fm\bar{3}m$ $FeMg_3$ is stable within the pressure range from 307 to 360 GPa. Our results reveal that this phase is stable <1590 GPa. At higher pressures, it will decompose into $FeMg_2$ and Fe. Phonon calculations show that it is dynamically unstable with low electron temperatures (see Fig. S8 in the Supplemental Material [32]), while at electronic temperatures of 8000 K, it becomes stable [see Fig. 5(d)].

C. Local packing motifs

In addition to the stable structures, we also predict hundreds of metastable structures in the Fe-Mg system up to 3 TPa. Since these are 0 K calculations, these low enthalpy metastable structures may become stable at elevated temperatures. In this respect, we also investigate the geometric features of those Fe_xMg_y phases with relative enthalpies (H_d) higher than the convex hull by 0.8 eV/atom (~9000 K) to reveal the overall structural behavior of the Fe-Mg system at high pressures. The cluster alignment method [41], which has successfully determined the crystal genes in crystals, glasses,

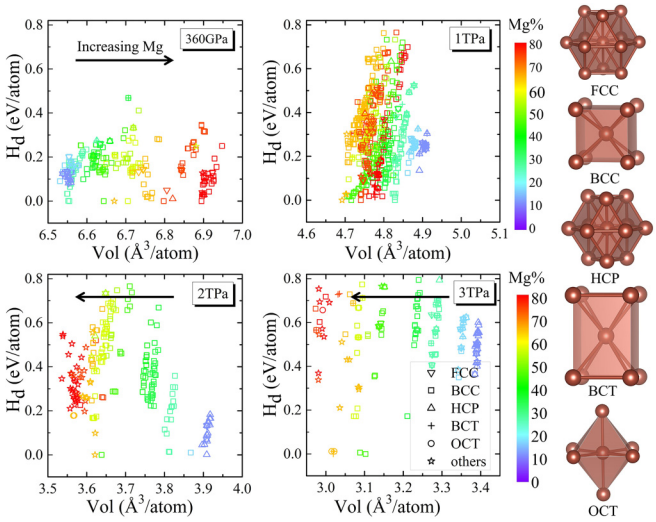

FIG. 6. The relative enthalpies (H_d) of low-enthalpy Fe_xMg_y structures as a function of their volumes, where the symbols represent the local packing motifs, the colors denote the atomic content of Mg. The local bonding states of the template motifs are shown on the right. The label "others" indicates a Fe-centered cluster with the lowest alignment scores of all five templates >0.125.

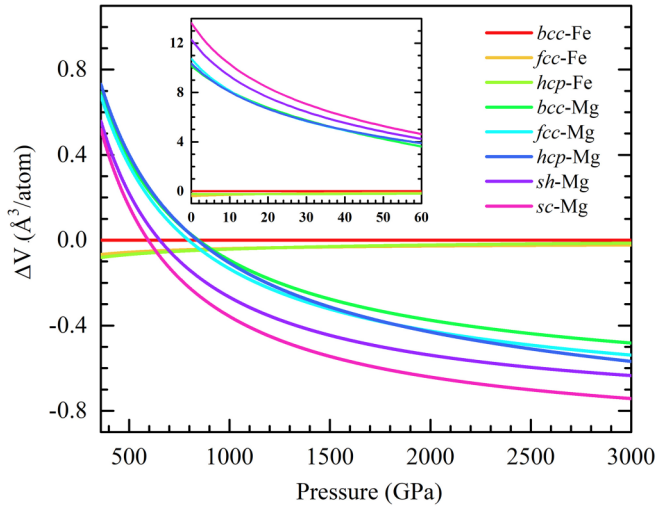

FIG. 7. Relative volume as a function of pressure for elementary Fe and Mg phases. The inset shows the same at low pressures.

and liquids, is adopted to identify the packing motifs of these structures. We first align the Fe-centered clusters as extracted from the low-enthalpy Fe_xMg_y phases against five template motifs, as shown in the right panel of Fig. 6. The template motifs include face-centered cubic, bcc, hcp, octahedron, and body-centered tetragonal, which are the most popular motifs found in the Fe-O [33] and Mg-O systems [30,42]. We can determine the building block of the structure in light of the alignment score, which describes the deviation of an as-extracted cluster from the perfect template. The alignment score criterion is set to be 0.125, allowing a small distortion of the ideal motifs of the crystal structures.

Figure 6 shows the relative enthalpies (H_d) of the stable and metastable phases with respect to the convex hull as functions of their volumes. Here, H_d is defined as the enthalpy above the convex hull with $H_d = 0$ denoting the ground states. The local packing motifs are indicated with different symbols, and colors represent the Mg fraction. As shown in Fig. 6, when Fe and Mg atomic fractions are comparable, most Fe_xMg_y phases tend to adopt a single bcc motif. With high Fe or Mg content, different structural motifs can coexist. At 360 GPa, the averaged atomic volume increases with increasing Mg concentration. However, at 2 and 3 TPa, the average atomic volumes decrease with increasing Mg concentration. At 1 TPa, different Mg concentrations lead to similar averaged atomic volumes.

To understand the change of volume-composition relations, we investigate the compression behavior of elementary Fe and Mg phases under ultrahigh pressures. We plot in Fig. 7 the pressure-volume relations for several Fe and Mg crystal structures. The solid lines are the fitting results of the third-order Birch-Murnaghan equation of state [43]. As shown in Fig. 7, all Fe allotropes have smaller atomic volume than Mg phases at pressures <600 GPa. In this range, the atomic volume difference between elementary Fe and Mg decreases with the increasing pressure. Then the volumes of the two elements become similar from 600 to 900 GPa. At pressures >900 GPa, the atomic volume of Fe allotropes become larger than those of Mg allotropes, and the volume difference increases with the increasing pressure. It is interesting to note that the atomic volume difference between Fe and Mg is more than one order of magnitude larger at ambient pressure than the one at ultrahigh pressures (see Fig. 7 inset). Such a dramatic change of Fe/Mg volume difference with respect to the pressure can explain the pressure-induced formation of Fe-Mg compounds. Under ambient pressure, the volume difference between Fe and Mg is so large that they are hardly miscible. With increasing pressure, Mg is more compressible than Fe, as evidenced by the volume difference reduction and volume crossover under pressure, leading to the formation of Fe-Mg compounds and different Fe-Mg motifs.

Our results suggest that stable stoichiometric Fe-Mg compounds should exist at extreme conditions of super-Earth interiors, whether in the solid cores of those with few Earth masses ($M_\oplus$) or the mantle of heavier ones with more than 8 $M_\oplus$ [35]. From 400 to 1600 GPa, abundant stoichiometric compounds and Mg-Fe solid solutions should exist because Fe and Mg have similar atomic volumes, promoting their intermixing. Above 1600 GPa, the atomic volume difference is significant, again decreasing their intersolubility. Only ε-Fe and bcc-like Fe_2Mg remain in Fe-rich stoichiometries, forming the basis for a eutectic subsystem in the cores of super-Earths with few Earth masses. Such highly pressure-dependent solubility behavior may result in super-Earth interiors with more complex layered structures than modeled so far [18].

IV. CONCLUSIONS

In summary, we identified several stable stoichiometric phases in the Fe-Mg system under exoplanetary interior pressures using the efficient AGA search method combined with DFT calculations. In addition to the stable structures, we

also predicted a significant number of metastable Fe_xMg_y structures with low enthalpies. The cluster alignment analysis reveals that all stable and metastable Fe-Mg compounds prefer a bcc packing motif at high pressures. In this paper, we provide a more comprehensive structure database to support future investigations of the high-pressure behavior of Fe-Mg compounds. However, to understand planetary cores, one must address the joint solubility of high-abundance elements in Fe, e.g., Mg, O, Si, H, and C, and their partitioning behavior between solid and melt, metal and silicate, etc. For this purpose, further investigation on the structural and thermodynamic behavior of ternary and quaternary systems involving high-abundance elements at terapascal pressures is in demand.

ACKNOWLEDGMENTS

Work at Xiamen University was supported by the National Natural Science Foundation of China (No. 11874307). Work at Iowa State University and Columbia University was supported by the National Science Foundation Awards No. EAR-1918134 and No. EAR-1918126. Work at Guangdong University of Technology was supported by the Guangdong Natural Science Foundation of China (Grants No. 2017B030306003 and No. 2019B1515120078).

[1] T. Massalski, H. Okamoto, P. R. Subramanian, and L. Kacprzak, *Binary alloy phase diagrams*, 2nd ed. (ASM International, Materials Park, 1990), 3542 pp.
[2] C. Jaouen, J. Delafond, N. Junqua, and P. Goudeau, Nucl. Instrum. Methods Phys. Res. B **43**, 34 (1989).
[3] E. P. Yelsukov, G. A. Dorofeev, and A. L. Ulyanov, Czech J. Phys. **55**, 913 (2005).
[4] N. Dubrovinskaia, L. Dubrovinsky, and C. McCammon, J. Phys.: Condens. Matter **16**, S1143 (2004).
[5] N. Dubrovinskaia, L. Dubrovinsky, I. Kantor, W. A. Crichton, V. Dmitriev, V. Prakapenka, G. Shen, L. Vitos, R. Ahuja, B. Johansson, and I. A. Abrikosov, Phys. Rev. Lett. **95**, 245502 (2005).
[6] K. Kadas, L. Vitos, B. Johansson, and R. Ahuja, Proc. Natl. Acad. Sci. USA **106**, 15560 (2009).
[7] Y. Li, L. Vočadlo, D. Alfè, and J. Brodholt, Phys. Earth Planet. Inter. **274**, 218 (2018).
[8] P. Gao, C. Su, S. Shao, S. Wang, P. Liu, S. Liu, and J. Lv, New J. Chem. **43**, 17403 (2019).
[9] D. M. Deaven and K. M. Ho, Phys. Rev. Lett. **75**, 288 (1995).
[10] S. M. Foiles, M. I. Baskes, and M. S. Daw, Phys. Rev. B **33**, 7983 (1986).
[11] A. Banerjea and J. R. Smith, Phys. Rev. B **37**, 6632 (1988).
[12] P. Brommer and F. Gahler, Philos. Mag. **86**, 753 (2006).
[13] P. Brommer and F. Gahler, Modell. Simul. Mater. Sci. Eng. **15**, 295 (2007).
[14] P. Giannozzi, S. Baroni, N. Bonini, M. Calandra, R. Car, C. Cavazzoni, D. Ceresoli, G. L. Chiarotti, M. Cococcioni, I. Dabo, A. Dal Corso, S. De Gironcoli, S. Fabris, G. Fratesi, R. Gebauer, U. Gerstmann, C. Gougoussis, A. Kokalj, M. Lazzeri, L. Martin-Samos *et al.*, J. Phys. Condens. Matter **21**, 395502 (2009).
[15] P. Giannozzi, O. Andreussi, T. Brumme, O. Bunau, M. Buongiorno Nardelli, M. Calandra, R. Car, C. Cavazzoni, D. Ceresoli, M. Cococcioni, N. Colonna, I. Carnimeo, A. Dal Corso, S. De Gironcoli, P. Delugas, R. A. Distasio, A. Ferretti, A. Floris, G. Fratesi, G. Fugallo *et al.*, J. Phys. Condens. Matter **29**, 465901 (2017).
[16] K. Umemoto, R. M. Wentzcovitch, Y. G. Yu, and R. Requist, Earth Planet. Sci. Lett. **276**, 198 (2008).
[17] K. Umemoto, R. M. Wentzcovitch, and P. B. Allen, Science **311**, 983 (2006).
[18] K. Umemoto, R. M. Wentzcovitch, S. Q. Wu, M. Ji, C. Z. Wang, and K. M. Ho, Earth Planet. Sci. Lett. **478**, 40 (2017).
[19] G. Shukla and R. M. Wentzcovitch, Phys. Earth Planet. Inter. **260**, 53 (2016).
[20] Y. Sun, M. Cococcioni, and R. M. Wentzcovitch, Phys. Rev. Materials **4**, 063605 (2020).
[21] C. G. Broyden, J. Inst. Maths Applies **6**, 222 (1970).
[22] C. G. Broyden, J. Inst. Maths Applies **6**, 76 (1970).
[23] D. Goldfarb, Math. Comput. **24**, 23 (1970).
[24] R. Fletcher, Comput. J. **13**, 317 (1970).
[25] D. F. Shanno, Math. Comp. **24**, 647 (1970).
[26] A. Togo, F. Oba, and I. Tanaka, Phys. Rev. B **78**, 134106 (2008).
[27] A. Togo and I. Tanaka, Scr. Mater. **108**, 1 (2015).
[28] W. A. Bassett and E. Huang, Science **238**, 780 (1987).
[29] A. Vattre and C. Denoual, J. Mech. Phys. Solids **92**, 1 (2016).
[30] Q. Zhu, A. R. Oganov, and A. O. Lyakhov, Phys. Chem. Chem. Phys. **15**, 7696 (2013).
[31] P. F. Li, G. Y. Gao, Y. C. Wang, and Y. M. Ma, J. Phys. Chem. C **114**, 21745 (2010).
[32] See Supplemental Material at http://link.aps.org/supplemental/10.1103/PhysRevB.104.144109 for crystallographic data, phonon spectras, and phase transition of $FeMg_2$ phases.
[33] G. L. Weerasinghe, C. J. Pickard, and R. J. Needs, J. Phys.: Condens. Matter **27**, 455501 (2015).
[34] S. Shao, W. J. Zhu, J. Lv, Y. C. Wang, Y. Chen, and Y. M. Ma, npj Comput. Mater. **6**, 11 (2020).
[35] A. P. van den Berg, D. A. Yuen, K. Umemoto, M. H. G. Jacobs, and R. M. Wentzcovitch, Icarus **317**, 412 (2019).
[36] K. Y. Sikka, Y. K. Vohra, and R. Chidambaram, Prog. Mater. Sci. **27**, 245 (1982).
[37] K. M. Ho, C. L. Fu, and B. N. Harmon, Phys. Rev. B **29**, 1575 (1984).
[38] G. J. Cuello, A. Fernández Cuillermet, G. B. Grad, R. E. Mayer, and J. R. Granada, J. Nucl. Mater. **218**, 236 (1995).
[39] G. B. Grad, P. Blaha, and J. Luitz, Phys. Rev. B **62**, 12743 (2000).
[40] Y. Lu, T. Sun, P. Zhang, P. Zhang, D. B. Zhang, and R. M. Wentzcovitch, Phys. Rev. Lett. **118**, 145702 (2017).
[41] Y. Sun, F. Zhang, Z. Ye, Y. Zhang, X. Fang, Z. Ding, C.-Z. Wang, M. I. Mendelev, R. T. Ott, M. J. Kramer, and K.-M. Ho, Sci. Rep. **6**, 23734 (2016).
[42] H. Niu, A. R. Oganov, X. Q. Chen, and D. Li, Sci. Rep. **5**, 18347 (2015).
[43] F. Birch, J. Geophys. Res. Solid Earth **83**, 1257 (1978).